Cell Reports

Report

Dynamic Remodeling of Pericytes *In Vivo* Maintains Capillary Coverage in the Adult Mouse Brain

Graphical Abstract

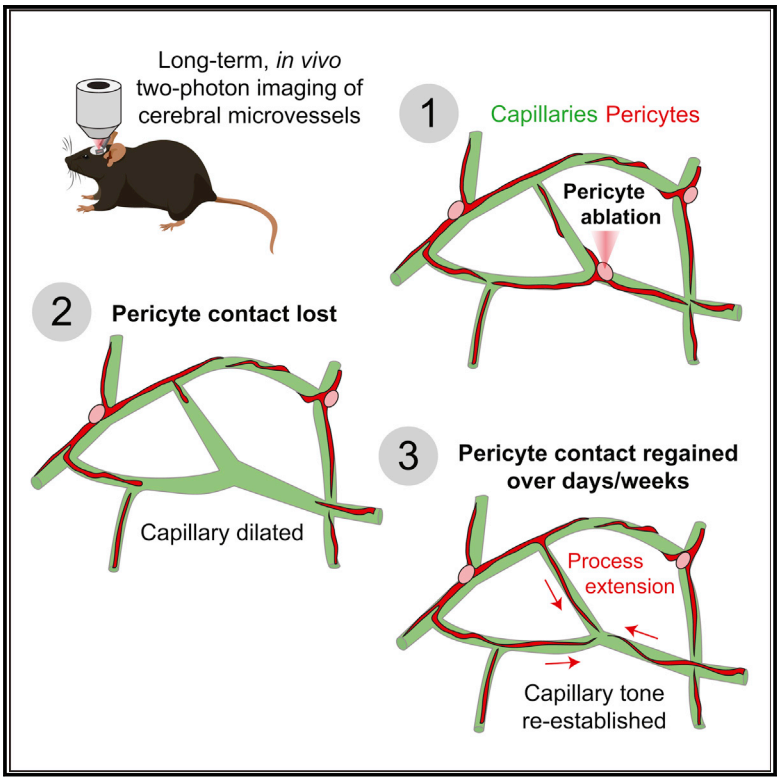

Authors

Andrée-Anne Berthiaume, Roger I. Grant, Konnor P. McDowell, ..., Manuel Levy, Narayan R. Bhat, Andy Y. Shih

Correspondence

shiha@musc.edu

In Brief

Pericyte-endothelial contact is important for many aspects of cerebrovascular health. Berthiaume et al. use longitudinal two-photon imaging to show that the processes of brain capillary pericytes are structurally plastic *in vivo*. Their processes can grow hundreds of micrometers to ensure contact with exposed endothelium following ablation of a single pericyte.

Highlights

- Brain capillary pericytes negotiate vascular territories with adjacent pericytes
- Pericytes can extend or retract their processes on the timescale of days
- Ablation of a pericyte evokes robust extension of processes from adjacent pericytes
- Loss of pericyte contact leads to local capillary dilation until contact is regained

Berthiaume et al., 2018, Cell Reports *22*, 8–16
January 2, 2018
https://doi.org/10.1016/j.celrep.2017.12.016

CellPress

OPEN ACCESS
CellPress

Cell Reports
Report

Dynamic Remodeling of Pericytes *In Vivo* Maintains Capillary Coverage in the Adult Mouse Brain

Andrée-Anne Berthiaume,[1] Roger I. Grant,[1] Konnor P. McDowell,[1] Robert G. Underly,[1] David A. Hartmann,[1] Manuel Levy,[1] Narayan R. Bhat,[1] and Andy Y. Shih[1,2,3,*]
[1]Department of Neuroscience
[2]Center for Biomedical Imaging
Medical University of South Carolina, Charleston, SC 29425, USA
[3]Lead Contact
*Correspondence: shiha@musc.edu
https://doi.org/10.1016/j.celrep.2017.12.016

SUMMARY

Direct contact and communication between pericytes and endothelial cells is critical for maintenance of cerebrovascular stability and blood-brain barrier function. Capillary pericytes have thin processes that reach hundreds of micrometers along the capillary bed. The processes of adjacent pericytes come in close proximity but do not overlap, yielding a cellular chain with discrete territories occupied by individual pericytes. Little is known about whether this pericyte chain is structurally dynamic in the adult brain. Using *in vivo* two-photon imaging in adult mouse cortex, we show that while pericyte somata were immobile, the tips of their processes underwent extensions and/or retractions over days. The selective ablation of single pericytes provoked exuberant extension of processes from neighboring pericytes to contact uncovered regions of the endothelium. Uncovered capillary regions had normal barrier function but were dilated until pericyte contact was regained. Pericyte structural plasticity may be critical for cerebrovascular health and warrants detailed investigation.

INTRODUCTION

Nearly a meter of vasculature is found in every cubic millimeter of cerebral cortex, and the vast majority is composed of capillaries (Blinder et al., 2013). The proper function of capillaries is crucial to brain health. Capillaries are the major site of nutrient delivery to support energy-intensive brain activity and also the primary location of the blood-brain barrier (BBB), which maintains the highly controlled environment needed for neural signaling (Zlokovic, 2008). Capillary walls are composed of endothelial cells, but their stability requires direct contact with pericytes, a specialized form of mural cell that resides in the basement membrane of the vessel (Sweeney et al., 2016). Pericytes and endothelial cells are physically linked through peg-and-socket interactions and communicate through a number of cell-contact-dependent and paracrine signaling pathways to control BBB integrity and the structure of the capillary network (Armulik et al., 2005).

Recent high-resolution optical imaging studies have shown that brain capillary pericytes are organized as a cellular chain along the capillary bed (Hartmann et al., 2015; Hill et al., 2015). Each pericyte extends thin, elongated processes from distinct ovoid somata to contact and communicate with multiple underlying endothelial cells (Allt and Lawrenson, 2001). Interestingly, the processes of neighboring pericytes are territorial and do not overlap in space. As such, each pericyte is a link within a chain. A breach in this chain would mean loss of endothelial contact and potential impairment of capillary function. This notion is based on a number of important studies showing that genetic manipulations leading to reduced pericyte coverage in the brain cause increased BBB leakage, abnormal vascular structure, endothelial hyperplasia, and neurodegeneration secondary to vascular deficits (Armulik et al., 2010; Bell et al., 2010; Ben-Zvi et al., 2014; Daneman et al., 2010; Hellström et al., 2001; Lindahl et al., 1997). Furthermore, cerebrovascular dysfunction is seen in pericyte-deficient mice that survive to adulthood, suggesting that pericytes continue to maintain vascular health following their integration and maturation at the capillary wall (Armulik et al., 2010; Bell et al., 2010). Critically, there is growing evidence that pericyte loss or dysfunction is involved in diseases that affect the adult human brain. For example, recent studies have shown reduced pericyte numbers in Alzheimer's disease (AD) (Miners et al., 2017; Sengillo et al., 2013) and cerebral autosomal dominant arteriopathy with subcortical infarcts and leukoencephalopathy (CADASIL) (Dziewulska and Lewandowska, 2012; Ghosh et al., 2015). In these diseases, the presumption is that pericytes develop normally but that accelerated pericyte loss with aging and pathology worsens BBB dysfunction and contributes to neurodegeneration. Pericyte death or migration from the vessel has also been reported after acute brain injuries such as stroke (Fernández-Klett et al., 2013; Hall et al., 2014) and trauma (Dore-Duffy et al., 2000). Thus, information on how pericyte-endothelial contact is regulated may lead to future therapies for improved cerebrovascular health in both chronic and acute brain pathologies.

Pericytes are known to be structurally plastic and motile during vascular development in the embryonic and perinatal brain (Hellström et al., 1999; Stapor et al., 2014). This property is important

to ensure that pericytes are properly organized within the vascular bed and that the endothelium is adequately covered. However, whether pericytes retain the ability to remodel and adapt to pericyte loss in the adult brain has yet to be investigated. Here, we address this question by directly visualizing the fine structure of capillary pericytes in the brains of live mice over days to weeks using *in vivo* two-photon microscopy. We find that, while pericyte somata are stable in location, their distal processes are dynamic. This active remodeling ensures pericyte-endothelial contact under basal conditions and acts to repair breaches in the pericyte chain following an insult.

RESULTS AND DISCUSSION

We imaged brain capillary pericytes in three inducible transgenic mouse lines, all of which exhibited bright fluorescent mural cells in the cerebrovasculature. In two of the mouse lines, mural cell-specific expression of the fluorescent protein, tdTomato, was achieved by cross-breeding a reporter line (Ai14) (Madisen et al., 2010) to mice expressing Cre recombinase under the control of neural/glial antigen 2 (NG2) (Zhu et al., 2011) or myosin heavy chain 11 (Myh11) (Wirth et al., 2008) promoters. These mice are hereafter referred to as NG2-tdTomato and Myh11-tdTomato, respectively. A single intraperitoneal injection of tamoxifen (100 mg/kg) to either mouse line led to sparse labeling of mural cells throughout the brain. The third transgenic mouse line achieved constitutive labeling of all mural cells through the cell-specific expression of yellow fluorescent protein (YFP) (Ai3) (Madisen et al., 2010) under the platelet-derived growth factor receptor β (PDGFRβ) promoter (Cuttler et al., 2011). We will refer to these as PDGFRβ-YFP mice. Chronic cranial imaging windows were generated in the skulls of these mice for optical access to the cerebral cortex during two-photon microscopy (Figures 1A and 1B). At each imaging session, we visualized endogenous tdTomato or YFP fluorescence from pericytes and green or red fluorescence from the vasculature, which was labeled through an intravenous (i.v.) injection of fluorescein isothiocyanate (FITC)-dextran or Texas red-dextrandye, respectively (Shih et al., 2012).

As in past studies, we observed a heterogeneity of mural cell types, ranging from ring-shaped smooth muscle cells on arterioles to pericytes with varying degrees of vessel coverage on pre-capillary arterioles and capillaries (Grant et al., 2017; Hartmann et al., 2015). In this study, we focused on pericytes adorning the mid-capillary regions (Figure 1C). These cells had round somata that protruded from the vessel wall and long, thin processes that coursed parallel along capillaries (Figures 1D and 1E). They were sparsely distributed because of their long processes and occupied the middle of the capillary bed. In a recent study, we showed that pericytes with these characteristics are negative for α-smooth muscle actin and that they can be distinguished from α-smooth muscle actin-positive pericytes/smooth muscle cells by examining capillary branches greater than fourth order from the penetrating arteriole (Grant et al., 2017).

Close inspection of *in vivo* images revealed instances where the tips of processes belonging to two neighboring capillary pericytes came within close proximity. Consistent with past work, the processes from two cells did not overlap in space along the same capillary branch (Hill et al., 2015). In fact, distinct gaps were occasionally observed between the processes of adjacent pericytes (Figure 1D). The presence of isolated pericytes allowed us to examine the full extent of processes extending from single cells (Figure 1E). The total length of processes extended by individual pericytes was, on average, 250 ± 41 μm (mean ± SD; n = 13 cells over 5 mice; 4 NG2-tdTomato and 1 Myh11-tdTomato), with a range of 194 μm to 315 μm. Thus, each individual pericyte covers an extensive amount of the underlying endothelium, mostly through contact with its processes. Further, as a collective, pericytes form a continuous, non-overlapping chain-like network along the entire capillary bed.

By repeatedly imaging the same animals over days to weeks, we were able to assess whether pericytes were stable in location and structure. We first measured the position of each pericyte soma over time, using a nearby capillary junction as a stable reference point, given the stability of the adult mouse cerebrovasculature (Harb et al., 2013) (Figures 1F and 1G). Over 14 cells, we observed no obvious change in soma position over ~50 days of imaging (Figure 1H). Thus, pericyte somata are stable in the normal adult brain. This finding is consistent with a recent longitudinal imaging study from another group (Cudmore et al., 2017).

We next examined the structure of processes extended by isolated capillary pericytes (Figures 2A–2C). Pericyte processes were separated into two groups, depending on whether the distal end of the branch was the end of the cell (terminal) or whether it bifurcated into further branches (non-terminal) (Figure 2D). Terminal processes were, on average, 44 ± 37 μm (mean ± SD; n = 46 processes over 15 cells from 6 mice; 5 NG2-tdTomato and 1 Myh11-tdTomato) in length, with a minimum and maximum of 2 μm and 132 μm, respectively. Non-terminal processes were similar in average length, 53 ± 26 μm (mean ± SD; n = 16 processes over 15 cells from 6 mice; 5 NG2-tdTomato and 1 Myh11-tdTomato), with a minimum and maximum of 19 μm and 115 μm, respectively.

Repeated imaging of the same pericytes revealed that non-terminal processes were stable in length over several weeks (Figures 2D–2F, blue) but that the distal tips of terminal processes often extended or retracted (Figures 2D, 2E, and 2G, pink). These changes in terminal process length occurred over the time course of days to weeks. Terminal processes did not remodel on a faster timescale of hours (Figures S1A and S1B). Extensions and retractions tended to move in one direction over the duration of imaging (up to 60 days), rather than fluctuate back and forth, though a few exceptions were noted (Figures S1C and S1D). Further, change in process length between imaging sessions appeared consistent over the entire duration of imaging, suggesting that imaging itself did not initiate a rapid phase of extension/retraction (Figures S1E and S1F). Over collated data, we observed that terminal processes were significantly more dynamic than non-terminal processes (Figures 2F and 2G). We found that 48% of terminal processes (31 of 64 processes over 23 cells from 6 mice; 5 NG2-tdTomato and 1 Myh11-tdTomato) exhibited length changes greater than 3 times the SD of change for non-terminal processes (Figure 2G). Dynamic terminal processes were broadly observed in our dataset, occurring in 19

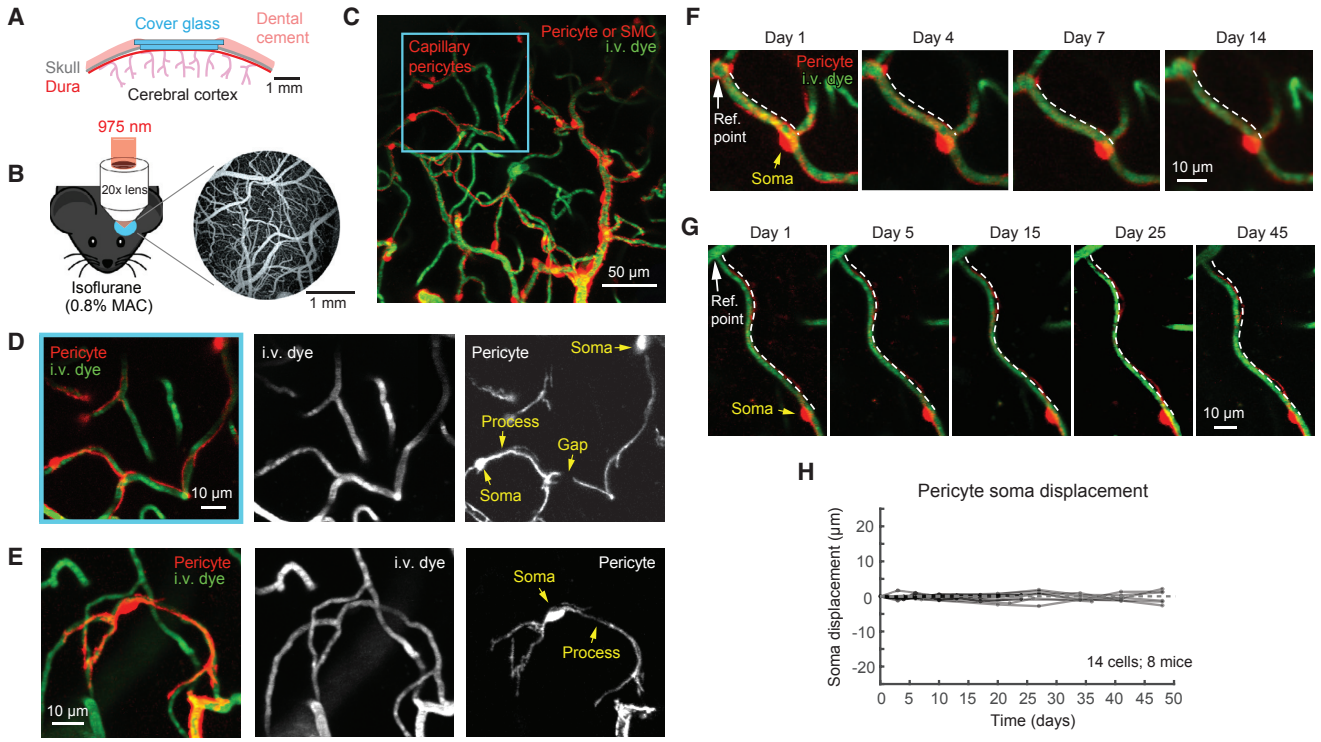

Figure 1. Chronic *In Vivo* Imaging of Capillary Pericytes with Two-Photon Microscopy

(A and B) A chronic skull-removed cranial imaging window was implanted over the left somatosensory cortex, and *in vivo* two-photon microscopy was performed under isoflurane anesthesia.

(C) Imaging through the cranial window reveals an intricate network of small vessels, labeled green with i.v. administered 2-MDa FITC-dextran (i.v. dye). Mural cells are labeled red through genetically expressed tdTomato. Image is from a Myh11-tdTomato mouse.

(D) High-resolution imaging allows for the visualization of detailed capillary pericyte structure (inset from C). The image highlights two pericyte somata from which arise several thin, elongated processes. Gaps between the processes of adjacent pericytes are also occasionally observed. This image is also used in Figure S2A.

(E) Representative image of an isolated pericyte. Image is from a Myh11-tdTomato mouse.

(F and G) Representative images of pericyte somata observed over time. Soma location was determined by measuring the distance from a stable capillary branchpoint (reference point) to the center of the pericyte soma. Images are from a NG2-tdTomato mouse (F) and a Myh11-tdTomato mouse (G).

(H) Compiled soma displacement measurements over time (n = 14 cells over 8 mice; 5 NG2-tdTomato and 3 Myh11-tdTomato).

of 23 cells, and 5 of the 6 mice examined (4 Ng2-tdTomato and 1 Myh11-tdTomato).

This finding raised the question of how fluctuations in terminal processes affected the territories of neighboring pericytes. In specific examples where there existed a discernible gap between pericytes, we could track the dynamic interplay of adjacent terminal process tips. We found that, as the process of one pericyte extended, the gap between cells would narrow and the process of the neighboring pericyte would eventually retract (Figure S2). Thus, neighboring pericytes appeared to negotiate their territories through complementary growth and retraction of terminal processes.

We next examined the consequence of losing one pericyte within the capillary pericyte chain. Several possible outcomes can be imagined. Pericytes may proliferate and/or migrate from other regions to cover the exposed endothelium. Nearby pericyte processes may extend to cover the exposed endothelium. Lastly, pericytes may not have the capacity to compensate for such a loss, leading to chronic endothelial exposure and potential capillary dysfunction. To explore this question, we used targeted two-photon irradiation to ablate single pericytes (Figure 3A) (Lou et al., 2016). This involved precise line scanning of the pericyte soma with higher laser powers at shorter wavelengths than observational imaging while avoiding damage to the adjacent capillary wall (Figure S3). Acute leakage of the 2-MDa FITC-dextran dye was not observed in the ablation experiments (with the exception of 1 out of 13 ablations exhibiting mild leakage; Figure S4B), suggesting that pericyte ablation could be reliably achieved without immediate incidental effects on the endothelium. Interestingly, ablation led to rapid loss of fluorescence throughout all cellular processes, though only the cell soma was irradiated (Figures 3A, S3A, and S3B; compare pre-ablation and 5 min post-ablation). Successfully ablated pericytes did not regain fluorescence at any post-imaging time point, indicating pericyte death rather than transient effects of photobleaching. Fortuitously, this effect unveiled the capillary territory occupied by the ablated pericyte, allowing the terminal processes of neighboring pericytes to be tracked over time.

Over the course of weeks following pericyte ablation, we observed an exuberant extension of terminal processes from

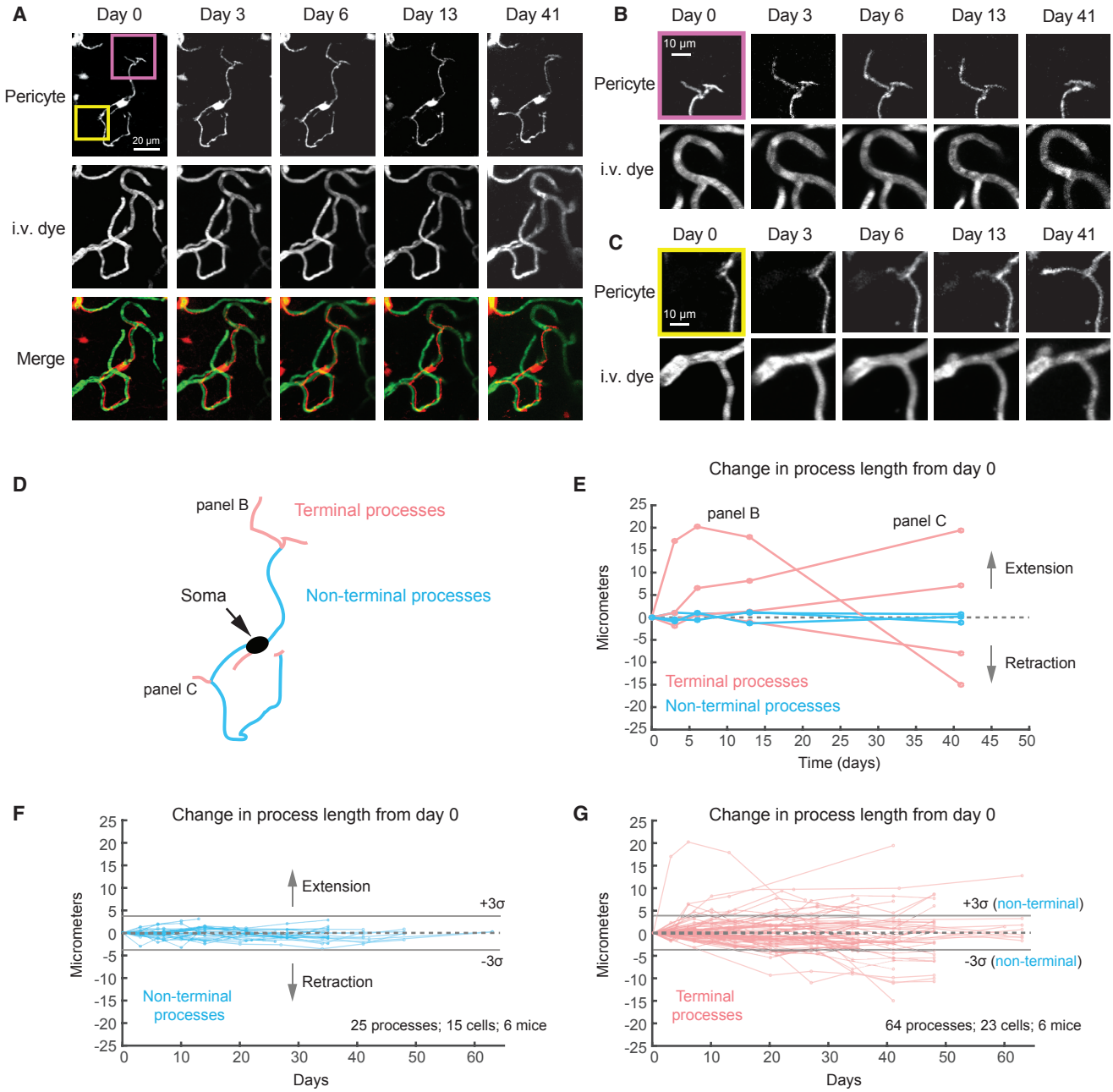

Figure 2. Structural Dynamics of Capillary Pericytes under Basal Conditions

(A) Longitudinal *in vivo* two-photon imaging of a single pericyte reveals the structural plasticity of pericytes processes, in contrast to the stability of the underlying blood vessels. Image is from a Myh11-tdTomato mouse.

(B) An inset of a process of interest, which extended beyond its baseline length over the course of 2 weeks and completely retracted by 41 days. No changes were observed in the structure of capillaries occupied by the pericyte.

(C) An inset of a second structurally dynamic process that extended along a stable capillary network over the course of 41 days.

(D) A schematic showing the distinction between terminal (pink) and non-terminal (blue) pericyte processes.

(E) Quantification of change in process lengths over time for the cell in (A)–(D).

(F) Composite data from all non-terminal processes tracked over time (n = 25 processes from 15 cells over 6 mice; 5 NG2-tdTomato and 1 Myh11-tdTomato).

(G) Composite data from all terminal processes tracked over time (n = 64 processes from 23 cells over 6 mice; 5 NG2-tdTomato and 1 Myh11-tdTomato). A ±3-SD range (3σ) for data from non-terminal processes is shown for statistical comparison with terminal process change.

See also Figures S1D, S1F, and S2.

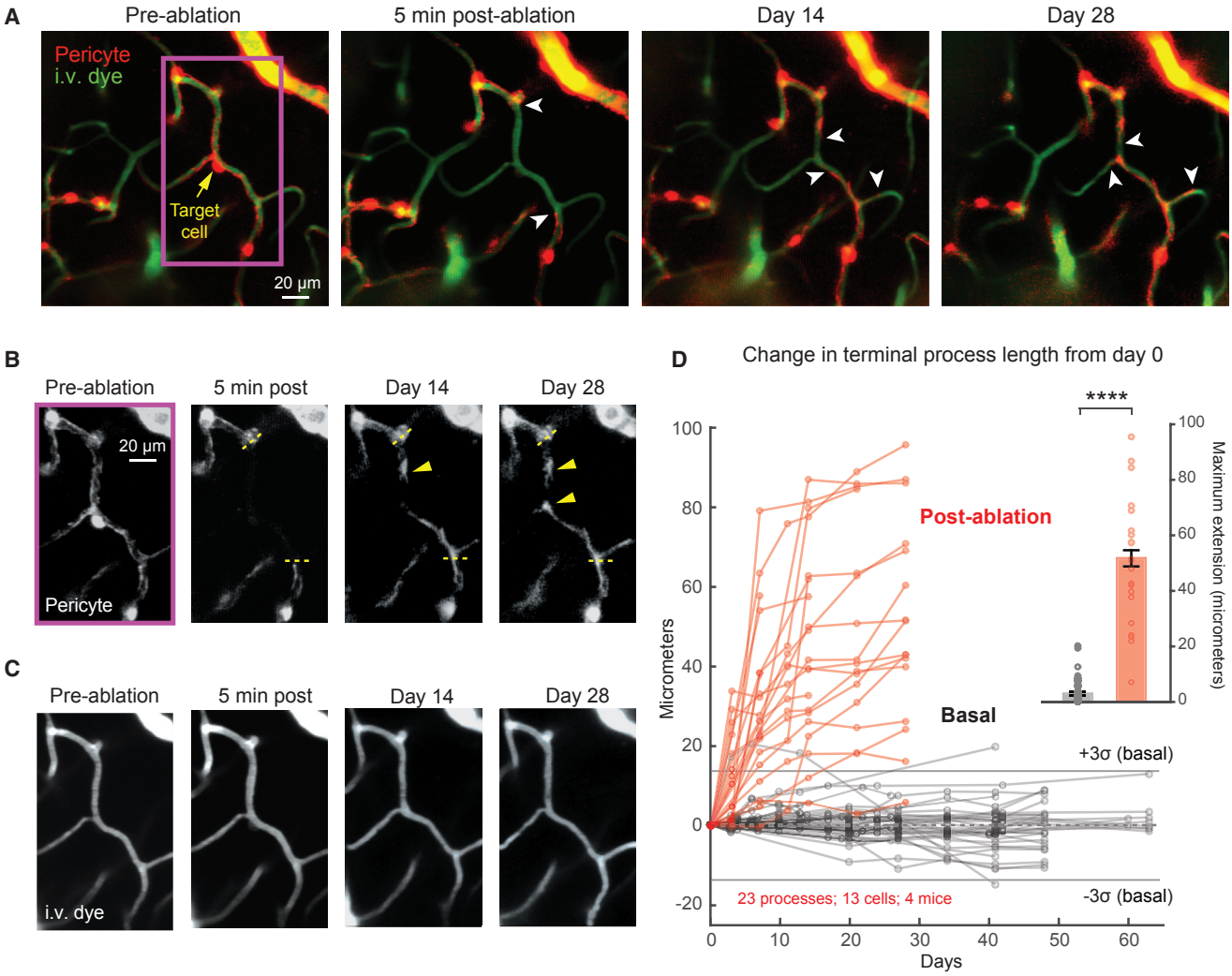

Figure 3. Robust Extension of Terminal Processes in Response to Ablation of a Single Pericyte

(A) Example of a single pericyte ablation experiment. The tracking of processes from neighboring pericytes over time revealed growth into the territory of the ablated cell (white arrowheads). Image is from a Myh11-tdTomato mouse. See also Figure S3.

(B) High-resolution images of the tdTomato channel showing pericyte structure over time. Yellow dotted line is boundary for domain of ablated pericyte. Yellow arrowheads highlight growth cone-like varicosities. See also Figure S4.

(C) High-resolution images of FITC-dextran channel showing stable capillary structure.

(D) Composite data of terminal process length change over time following the ablation of a single pericyte (red). A ±3-SD range (3σ) for data from terminal processes under basal conditions (black; from Figure 2G) is shown for statistical comparison with terminal process length change after ablation. An inset graph compares maximum distances of process extension in basal and post-ablation groups. ****$p < 0.0001$, unpaired t test; $t(85) = 16.17$; $n = 64$ terminal processes for basal conditions, and $n = 23$ terminal processes of neighboring pericytes from 13 ablation experiments over 4 mice; 1 NG2-tdTomato, 2 Myh11-tdTomato, and 1 PDGFRβ-YFP. Data are presented as mean ± SEM.

neighboring pericytes into the exposed region of the endothelium (Figures 3A–3C and S4). In the most rapid phase of growth, i.e., within the first 10 days after ablation, some processes extended up to ~60 to 80 μm, corresponding to a growth rate of ~6 to 8 μm per day (Figure 3D, red traces). This is compared to a typical maximal rate of extension under basal conditions of ~0.5 μm per day (Figure 3D, gray traces). Nearly all processes examined (96%; 22 of 23 terminal processes over 13 cells from 4 mice; 1 NG2-tdTomato, 2 Myh11-tdTomato, and 1 PDGFRβ-YFP) extended more than 3 times the SD range for terminal processes under basal conditions. Further, the maximal distance of extension was 10 times greater after ablation, compared to those observed under basal conditions (Figure 3D, inset).

We observed that only extensions, and not retractions, occurred after ablation. The extensions appeared to grow until the entirety of the exposed endothelium was contacted by a pericyte. This is evident in the example in Figures 3A and 3B, where the ablated pericyte exposed an ~100-μm length of capillary, and the processes of neighboring pericytes extended into nearly the entire region within 28 days. However, the completeness of

coverage could not always be ascertained, as one flanking pericyte was sometimes not genetically labeled or insufficiently fluorescent for reliable quantification. Interestingly, we occasionally observed bright varicosities at the tip of the extending terminal process, suggesting the presence of a growth cone-like structure (Figure 3B, yellow arrowheads; Figures S4A and S4B). Further, it appeared that growing processes involved the addition of new cytoplasmic volume to the pericyte, as processes elsewhere on the same cell did not retract proportionally to conserve cell size (Figure S4C).

After pericyte ablation, we generally did not observe new formation or elimination of capillary branches. The exception was one ablation experiment out of 13 that involved slightly more acute vascular damage during pericyte ablation (noted earlier), where a newly formed capillary branch could later be seen at the site of ablation (Figure S4B, i.v. dye channel; 21 and 28 days post-ablation). This overall lack of vascular remodeling was somewhat surprising, since the disruption of pericyte endothelial interaction is known to cause endothelial hyperplasia (Hellström et al., 1999). However, this may mean that greater numbers of pericytes need to be lost before capillary remodeling occurs. While vascular branching was largely unchanged, we noticed that uncovered capillary segments were consistently more dilated in the first weeks post-ablation (Figures 4A–4C). This dilation was unlikely to be a product of acute light or heat exposure, since it remained evident up to 14 days after pericyte ablation, and all capillary measurements were taken at locations away from soma ablation sites. Furthermore, as neighboring pericytes extended to reestablish contact with these regions, capillary lumen diameter returned to a state of partial constriction (Figures 4D and 4E). This suggests that pericyte contact may either directly or indirectly promote the development of basal capillary tone.

Finally, we examined whether BBB integrity was compromised at capillary regions uncovered by pericytes. A bolus of low-molecular-weight dye (Alexa Fluor 647 cadaverine; ~1 kDa molecular weight [MW]) was injected i.v. during image capture to detect potential dye extravasation into the surrounding parenchyma. Alexa Fluor-conjugated cadaverine is known to cross the leaky BBB of pericyte-deficient mice, where the major route of leakage was endothelial transcytosis (Armulik et al., 2010). Thus, both transcellular and paracellular leakage, which is less selective to tracer type, should be detectable with Alexa Fluor 647 cadaverine. We first tested our sensitivity to BBB leakage using this approach by performing a positive control where ablative line scans were used to directly induce capillary injury (4 locations over 3 mice; 1 NG2-tdTomato and 2 PDGFRβ-YFP) (Lou et al., 2016) (Figures 4F and 4G). This injury led to a 12-fold increase in parenchymal fluorescence following bolus injection, compared to a bolus injection pre-injury. Surprisingly, when the same method was used to examine uncovered capillaries after pericyte ablation, we did not observe significant increases in parenchymal fluorescence either 5 min or 2 days following ablation (6 locations over 4 mice; 1 NG2-tdTomato, 1 Myh11-tdTomato, and 2 PDGFRβ-YFP) (Figures 4H and 4I). This lack of BBB leakage may be due to preserved endothelial health through paracrine signals from neighboring pericytes or microglial-dependent closure of the BBB (Lou et al., 2016).

Our longitudinal imaging studies have revealed pericyte plasticity in the adult brain. Individual pericytes negotiate their capillary territories with neighboring pericytes through extensions and retractions of terminal processes. In the face of pericyte loss, as may occur during normal aging or at an accelerated rate in vascular dementia and brain injury, pericytes can actively adapt to ensure endothelial coverage by extending their wide-reaching processes. This result holds true across studies using three different mural-cell Cre drivers, suggesting that structural plasticity is a common attribute of mid-capillary pericytes. Pericyte-endothelial contact is critical for many vascular homeostatic functions, and it remains to be seen how modulation of pericyte structural plasticity on a broad level affects cerebral blood flow regulation, metabolite exchange, BBB integrity, and microvascular architecture. Whether capillary pericytes are involved in cerebral blood flow regulation is controversial (Attwell et al., 2016; Hill et al., 2015; Kisler et al., 2017). Our data suggest that pericyte loss leads to capillary dilation under basal conditions, which may decrease capillary flow resistance and alter metabolic exchange. While we did not observe BBB disruption or change in vascular architecture, it is likely that a higher degree of pericyte loss is needed to perturb these critical cerebrovascular features. These findings also raise the question of whether pericyte structural plasticity is decreased with age or in cerebrovascular disease, which would limit the ability of remaining pericytes to compensate for pericyte loss.

Under basal conditions, the pull-push exchange of territory between neighboring pericytes might involve the secretion of pericyte-derived repulsive signals, akin to semaphorins during neuronal axon guidance. Ablation of one pericyte would then relieve the inhibition of neighboring pericytes, allowing cell growth to occur. Endothelial-derived signals that promote pericyte recruitment during development, such as PDGFB and transforming growth factor β (TGFβ) (Armulik et al., 2011), may augment and guide pericyte process growth in the adult brain. Indeed, stimulating PDGFB/PDGFRβ signaling in adults can promote vascular maturation and stability as well as reduce bleeding in peripheral tissues (Lebrin et al., 2010). Further studies of how these signaling pathways affect pericyte structural plasticity may yield novel approaches to combat cerebrovascular dysfunction during brain injury and age-related brain disease.

EXPERIMENTAL PROCEDURES

Mice

TdTomato reporter mice (Ai14) on a C57BL/6 background were purchased from Jackson Laboratory (stock no. 007914) (Madisen et al., 2010). These mice were bred with two different inducible Cre driver lines to achieve sparsely labeled pericytes: NG2-CreER mice (Jackson Laboratory stock no. 008538) (Zhu et al., 2011) and Myh11-CreERT2 mice (Jackson Laboratory stock no. 019079). In a subset of pericyte ablation and BBB leakage experiments, we crossed constitutive PDGFRβ-Cre mice (Cuttler et al., 2011) with a YFP reporter line (Ai3) (Jackson Laboratory stock no. 007903) (Madisen et al., 2010) to express YFP in all mural cells. Mice were maintained in standard cages on a 12-hr:12-hr light:dark cycle and housed 5 or fewer per cage. Following cranial window implantation, mice were housed singly. Both male and female mice were used, and all mice used were between 5 to 7 months of age at the start of imaging. The Institutional Animal Care and Use Committee at the Medical University of South Carolina approved the procedures used in this study.

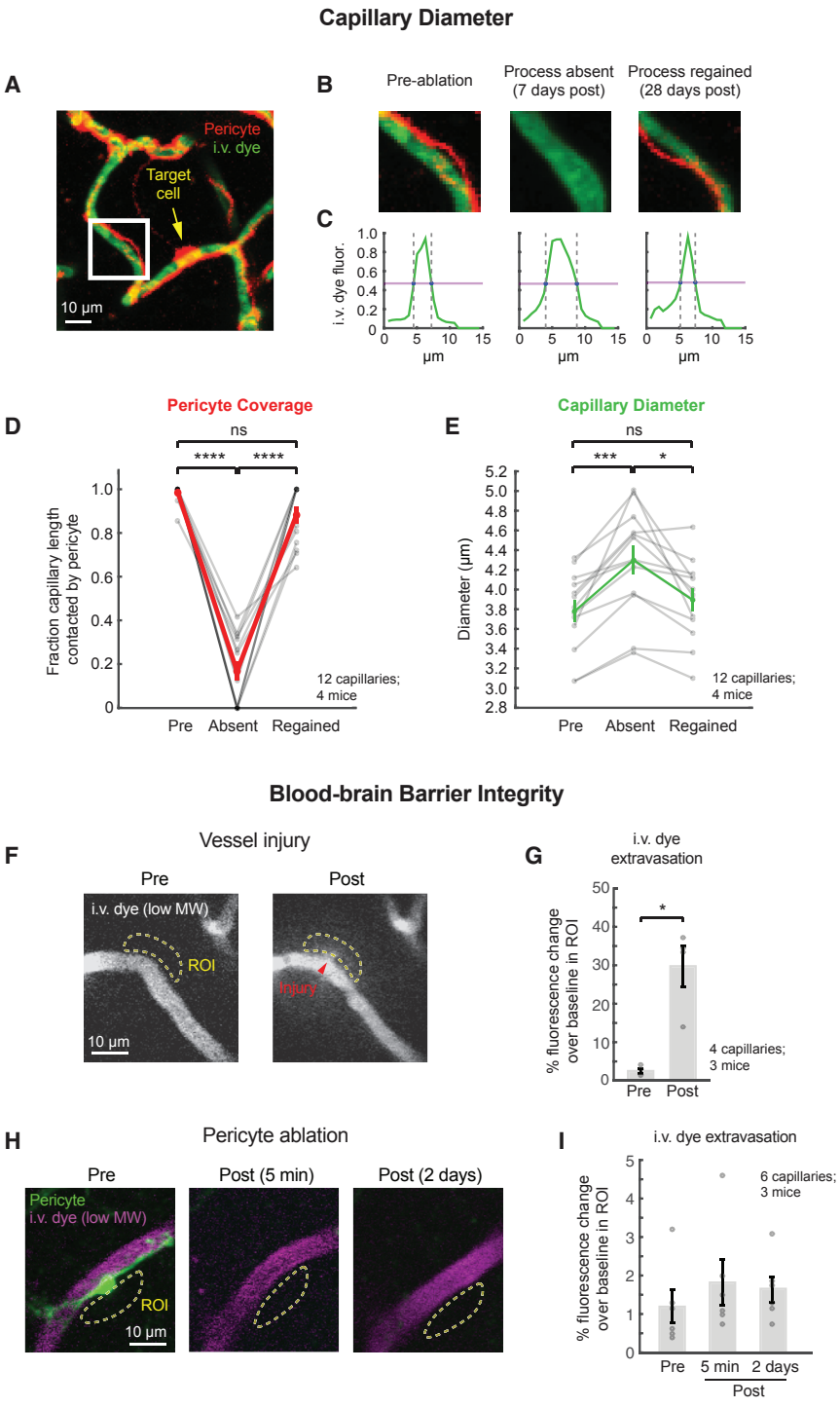

Figure 4. Capillary Changes following Pericyte Ablation

(A) Image of capillaries covered by a pericyte targeted for ablation from a Myh11-tdTomato mouse.

(B) Inset region shows a capillary segment measured before pericyte ablation and at 7 and 28 days post-ablation. See Figure S4A for extended images.

(C) Normalized fluorescence intensity profiles collected across the capillary width (green) were used to calculate capillary diameter at half maximum (purple line) at each time point.

(D and E) Plot of pericyte coverage (D) and capillary diameter (E) over time. For each capillary segment, three time points were sampled: one pre-ablation time point, one post-ablation time point where pericyte coverage of the capillary was completely or partially absent (selections ranged between 3 and 14 days), and one subsequent post-ablation time point where pericyte coverage was completely or partially regained (selections ranged between 7 and 28 days). For pericyte coverage, $p < 0.0001$; main effect, $F(1.591, 19.1) = 136.8$, one-way ANOVA with repeated measures. ****$p < 0.0001$ for Tukey post hoc test. ns, non-significant. For vessel diameter, $p < 0.0001$; main effect, $F(1.702, 18.72) = 16.76$, one-way ANOVA with repeated measures. ***$p < 0.001$, *$p < 0.05$ for Tukey post hoc test. N = 12 pericyte ablations or capillaries from 4 mice; 1 NG2-tdTomato, 2 Myh11-tdTomato, and 1 PDGFRβ-YFP. Red and green lines indicate mean ± SEM.

(F) Example images during an i.v. bolus injection of Alexa Fluor 647 cadaverine to assess BBB integrity once before and once after line-scan-induced capillary injury. Image is from a NG2-tdTomato mouse.

(G) Average Alexa Fluor 647 fluorescence change over baseline (fluorescence prior to bolus injection) in ROIs placed immediately adjacent to the pre-injury and injured capillary. *$p < 0.05$, paired t test; $t(3) = 5.305$. n = 4 capillaries). N = 4 capillaries from 3 mice; 1 NG2-tdTomato and 2 PDGFRβ-YFP. Data are presented as mean ± SEM.

(H) Example images during an i.v. bolus injection of Alexa Fluor 647 cadaverine before and after targeted pericyte ablation. Image is from a PDGFRβ-YFP mouse.

(I) Average Alexa Fluor 647 fluorescence change over baseline in ROIs placed immediately adjacent to capillary. $p = 0.45$, main effect, one-way ANOVA with repeated measures. N = 6 pericyte ablations or capillaries from 3 mice; 1 NG2-tdTomato and 2 PDGFRβ-YFP. Data are presented as mean ± SEM.

Surgery

See the Supplemental Experimental Procedures.

Experimental Timeline

To induce tdTomato expression, a single dose of tamoxifen (T5648; Sigma-Aldrich), dissolved in corn oil:ethanol (9:1), was injected intraperitoneally at a dose of 100 mg/kg approximately 2 weeks prior to the start of imaging. *In vivo* imaging sessions commenced no earlier than 3 weeks after cranial window implantation to ensure that all surgically caused inflammation had resolved, and they continued at approximately twice per week for up to 7 weeks. The exact imaging timeline varied across animals, as the optimal timescale to visualize pericyte structural plasticity had not yet been established at the outset of these studies.

In Vivo Two-Photon Microscopy

Our procedures for *in vivo* two-photon imaging have been described previously (Shih et al., 2012). Additional details are provided in the Supplemental Experimental Procedures.

Two-Photon Thermal Ablation

For ablation of individual pericytes between 50 to 200 μm below the pial surface, we applied line scans (~50 mW, 725 nm) to the target pericyte somata. Line scanning was maintained for 60 to 90 s, with approximately 100 pixels scanned across the soma per line scan cycle and a pixel dwell time of 1 μs. This procedure led to rapid loss of tdTomato fluorescence throughout the entire pericyte. The ablated cell was then re-imaged after 2 to 3 days to confirm permanent cell ablation. If the cell regained any amount of tdTomato fluorescence, the ablation was deemed unsuccessful, and the experiment was omitted from quantification. With successful ablation, the targeted pericyte did not regain fluorescence at any post-ablation time point. With the exception of one mouse, completely different sets of mice were used for basal imaging versus pericyte ablation experiments.

Quantification of Pericyte Morphometrics

Length of pericyte processes was measured in 3 dimensions using the Simple Neurite Tracer ImageJ plug-in. Each process measurement was obtained three separate times and averaged to reduce measurement variability. Measurements of soma location over time and pericyte process diameter were taken manually in 2 dimensions using the ImageJ line selection tool. These quantifications were also taken as an average of 3 separate measurements. Length measurements were not made in a blinded fashion in these studies.

Quantification of Capillary Diameter

The diameter of capillaries was quantified from maximally projected images. Custom MATLAB code was used to measure full width at half maximum (FWHM) of the fluorescence intensity profile across the vessel lumen width as described previously, with some modifications (Shih et al., 2012). FWHM was calculated from 10 evenly spaced locations (~2 μm spacing) along the length of the capillary of interest. These 10 width measurements were then averaged to provide a single lumen diameter value before and at two time points after pericyte ablation. This approach was taken to reduce measurement bias and to obtain more accurate overall diameter measurements (Ivanova et al., 2017).

Quantification of BBB Leakage

During continuous imaging, a single 50-μL bolus of 400 μM Alexa Fluor 647 cadaverine dye (A30679; Thermo Fisher Scientific) was injected through the retro-orbital vein. To avoid light contamination, a 740-nm fiber-coupled LED (M28L01, M740F2: Thorlabs) was used to guide the dye injection while the animal was within the microscope light box. Alexa Fluor 647 was excited at 825 nm, and emission was collected with an ET655/40m filter. Images were collected at a frame rate of 2.91 frames per second (fps). Fluorescence intensity change in movies was measured using ImageJ by drawing regions of interest (ROIs) directly on a capillary, to detect the time of dye influx, and in the parechyma immediately adjacent to the capillary to detect extravasated dye. An average of fluorescence values from 0 to 3.5 s after the arrival of the dye at the imaging location was compared to average fluorescence values in the same location prior to dye injection, i.e., at baseline. Bolus injections were made and dye extravasation examined once before pericyte ablation, as well as 5 min and 2 days post-ablation. For the induction of capillary injury as a positive control, we applied line scans across the capillary wall for 90 to 120 s at a laser power of 50 to 85 mW at 725 nm. Bolus injections were made and dye extravasation measured at a pre-injury and a post-injury time point.

Statistics

Statistical analyses were performed using GraphPad Prism software. Statistical tests and details are provided in the figure legends. Tests of normality were first performed to validate the use of parametric tests.

SUPPLEMENTAL INFORMATION

Supplemental Information includes Supplemental Experimental Procedures and four figures and can be found with this article online at https://doi.org/10.1016/j.celrep.2017.12.016.

ACKNOWLEDGMENTS

We thank Chase J. Burton, Vanessa Coelho-Santos, and Ashley N. Watson for helpful discussions. This work was supported by grants to A.Y.S. from NIH/NINDS (NS085402 and NS096997), NIH/NIGMS (P20GM12345), NSF (1539034), the American Heart Association (14GRNT20480366), and an Alzheimer's Association NIRG award (2016-NIRG-397149). N.R.B. is supported by the NIH/NIA (AG052321). R.I.G. is supported by NIH R25 (GM113278-01). D.A.H. is supported by NIH T32 (GM08716), NIH/NCATS (UL1 TR001450 and TL1 TR001451), and NIH/NINDS F30 (NS096868).

AUTHOR CONTRIBUTIONS

A.A.B. designed and executed all imaging studies. A.A.B., R.I.G., K.P.M., and A.Y.S. performed data analysis. R.G.U., D.A.H., M.L., and N.R.B. provided help with experimental design, surgery, and animal husbandry. A.A.B. and A.Y.S. wrote the manuscript, with feedback from all other authors.

DECLARATION OF INTERESTS

The authors declare no competing interests.

Received: July 25, 2017
Revised: November 1, 2017
Accepted: December 3, 2017
Published: January 2, 2018

REFERENCES

Allt, G., and Lawrenson, J.G. (2001). Pericytes: cell biology and pathology. Cells, Tissue, Organs *169*, 1–11.

Armulik, A., Abramsson, A., and Betsholtz, C. (2005). Endothelial/pericyte interactions. Circ. Res. *97*, 512–523.

Armulik, A., Genové, G., Mäe, M., Nisancioglu, M.H., Wallgard, E., Niaudet, C., He, L., Norlin, J., Lindblom, P., Strittmatter, K., et al. (2010). Pericytes regulate the blood-brain barrier. Nature *468*, 557–561.

Armulik, A., Genové, G., and Betsholtz, C. (2011). Pericytes: developmental, physiological, and pathological perspectives, problems, and promises. Dev. Cell *21*, 193–215.

Attwell, D., Mishra, A., Hall, C.N., O'Farrell, F.M., and Dalkara, T. (2016). What is a pericyte? J. Cereb. Blood Flow Metab. *36*, 451–455.

Bell, R.D., Winkler, E.A., Sagare, A.P., Singh, I., LaRue, B., Deane, R., and Zlokovic, B.V. (2010). Pericytes control key neurovascular functions and neuronal phenotype in the adult brain and during brain aging. Neuron *68*, 409–427.

Ben-Zvi, A., Lacoste, B., Kur, E., Andreone, B.J., Mayshar, Y., Yan, H., and Gu, C. (2014). Mfsd2a is critical for the formation and function of the blood-brain barrier. Nature *509*, 507–511.

Blinder, P., Tsai, P.S., Kaufhold, J.P., Knutsen, P.M., Suhl, H., and Kleinfeld, D. (2013). The cortical angiome: an interconnected vascular network with noncolumnar patterns of blood flow. Nat. Neurosci. *16*, 889–897.

Cudmore, R.H., Dougherty, S.E., and Linden, D.J. (2017). Cerebral vascular structure in the motor cortex of adult mice is stable and is not altered by voluntary exercise. J. Cereb. Blood Flow Metab. *37*, 3725–3743.

Cuttler, A.S., LeClair, R.J., Stohn, J.P., Wang, Q., Sorenson, C.M., Liaw, L., and Lindner, V. (2011). Characterization of Pdgfrb-Cre transgenic mice reveals reduction of ROSA26 reporter activity in remodeling arteries. Genesis *49*, 673–680.

Daneman, R., Zhou, L., Kebede, A.A., and Barres, B.A. (2010). Pericytes are required for blood-brain barrier integrity during embryogenesis. Nature *468*, 562–566.

Dore-Duffy, P., Owen, C., Balabanov, R., Murphy, S., Beaumont, T., and Rafols, J.A. (2000). Pericyte migration from the vascular wall in response to traumatic brain injury. Microvasc. Res. *60*, 55–69.

Dziewulska, D., and Lewandowska, E. (2012). Pericytes as a new target for pathological processes in CADASIL. Neuropathology *32*, 515–521.

Fernández-Klett, F., Potas, J.R., Hilpert, D., Blazej, K., Radke, J., Huck, J., Engel, O., Stenzel, W., Genové, G., and Priller, J. (2013). Early loss of pericytes and perivascular stromal cell-induced scar formation after stroke. J. Cereb. Blood Flow Metab. *33*, 428–439.

Ghosh, M., Balbi, M., Hellal, F., Dichgans, M., Lindauer, U., and Plesnila, N. (2015). Pericytes are involved in the pathogenesis of cerebral autosomal dominant arteriopathy with subcortical infarcts and leukoencephalopathy. Ann. Neurol. *78*, 887–900.

Grant, R.I., Hartmann, D.A., Underly, R.G., Berthiaume, A.A., Bhat, N.R., and Shih, A.Y. (2017). Organizational hierarchy and structural diversity of microvascular pericytes in adult mouse cortex. J. Cereb. Blood Flow Metab., X17732229, Published online January 1, 2017. https://doi.org/10.1177/0271678X17732229.

Hall, C.N., Reynell, C., Gesslein, B., Hamilton, N.B., Mishra, A., Sutherland, B.A., O'Farrell, F.M., Buchan, A.M., Lauritzen, M., and Attwell, D. (2014). Capillary pericytes regulate cerebral blood flow in health and disease. Nature *508*, 55–60.

Harb, R., Whiteus, C., Freitas, C., and Grutzendler, J. (2013). In vivo imaging of cerebral microvascular plasticity from birth to death. J. Cereb. Blood Flow Metab. *33*, 146–156.

Hartmann, D.A., Underly, R.G., Grant, R.I., Watson, A.N., Lindner, V., and Shih, A.Y. (2015). Pericyte structure and distribution in the cerebral cortex revealed by high-resolution imaging of transgenic mice. Neurophotonics *2*, 041402.

Hellström, M., Kalén, M., Lindahl, P., Abramsson, A., and Betsholtz, C. (1999). Role of PDGF-B and PDGFR-beta in recruitment of vascular smooth muscle cells and pericytes during embryonic blood vessel formation in the mouse. Development *126*, 3047–3055.

Hellström, M., Gerhardt, H., Kalén, M., Li, X., Eriksson, U., Wolburg, H., and Betsholtz, C. (2001). Lack of pericytes leads to endothelial hyperplasia and abnormal vascular morphogenesis. J. Cell Biol. *153*, 543–553.

Hill, R.A., Tong, L., Yuan, P., Murikinati, S., Gupta, S., and Grutzendler, J. (2015). Regional blood flow in the normal and ischemic brain is controlled by arteriolar smooth muscle cell contractility and not by capillary pericytes. Neuron *87*, 95–110.

Ivanova, E., Kovacs-Oller, T., and Sagdullaev, B.T. (2017). Vascular pericyte impairment and connexin43 gap junction deficit contribute to vasomotor decline in diabetic retinopathy. J. Neurosci. *37*, 7580–7594.

Kisler, K., Nelson, A.R., Rege, S.V., Ramanathan, A., Wang, Y., Ahuja, A., Lazic, D., Tsai, P.S., Zhao, Z., Zhou, Y., et al. (2017). Pericyte degeneration leads to neurovascular uncoupling and limits oxygen supply to brain. Nat. Neurosci. *20*, 406–416.

Lebrin, F., Srun, S., Raymond, K., Martin, S., van den Brink, S., Freitas, C., Bréant, C., Mathivet, T., Larrivée, B., Thomas, J.L., et al. (2010). Thalidomide stimulates vessel maturation and reduces epistaxis in individuals with hereditary hemorrhagic telangiectasia. Nat. Med. *16*, 420–428.

Lindahl, P., Johansson, B.R., Levéen, P., and Betsholtz, C. (1997). Pericyte loss and microaneurysm formation in PDGF-B-deficient mice. Science *277*, 242–245.

Lou, N., Takano, T., Pei, Y., Xavier, A.L., Goldman, S.A., and Nedergaard, M. (2016). Purinergic receptor P2RY12-dependent microglial closure of the injured blood-brain barrier. Proc. Natl. Acad. Sci. USA *113*, 1074–1079.

Madisen, L., Zwingman, T.A., Sunkin, S.M., Oh, S.W., Zariwala, H.A., Gu, H., Ng, L.L., Palmiter, R.D., Hawrylycz, M.J., Jones, A.R., et al. (2010). A robust and high-throughput Cre reporting and characterization system for the whole mouse brain. Nat. Neurosci. *13*, 133–140.

Miners, J.S., Schulz, I., and Love, S. (2017). Differing associations between Aβ accumulation, hypoperfusion, blood-brain barrier dysfunction and loss of PDGFRB pericyte marker in the precuneus and parietal white matter in Alzheimer's disease. J. Cereb. Blood Flow Metab., X17690761, Published January 1, 2017. https://doi.org/10.1177/0271678X17690761.

Sengillo, J.D., Winkler, E.A., Walker, C.T., Sullivan, J.S., Johnson, M., and Zlokovic, B.V. (2013). Deficiency in mural vascular cells coincides with blood-brain barrier disruption in Alzheimer's disease. Brain Pathol. *23*, 303–310.

Shih, A.Y., Driscoll, J.D., Drew, P.J., Nishimura, N., Schaffer, C.B., and Kleinfeld, D. (2012). Two-photon microscopy as a tool to study blood flow and neurovascular coupling in the rodent brain. J. Cereb. Blood Flow Metab. *32*, 1277–1309.

Stapor, P.C., Sweat, R.S., Dashti, D.C., Betancourt, A.M., and Murfee, W.L. (2014). Pericyte dynamics during angiogenesis: new insights from new identities. J. Vasc. Res. *51*, 163–174.

Sweeney, M.D., Ayyadurai, S., and Zlokovic, B.V. (2016). Pericytes of the neurovascular unit: key functions and signaling pathways. Nat. Neurosci. *19*, 771–783.

Wirth, A., Benyó, Z., Lukasova, M., Leutgeb, B., Wettschureck, N., Gorbey, S., Orsy, P., Horváth, B., Maser-Gluth, C., Greiner, E., et al. (2008). G12-G13-LARG-mediated signaling in vascular smooth muscle is required for salt-induced hypertension. Nat. Med. *14*, 64–68.

Zhu, X., Hill, R.A., Dietrich, D., Komitova, M., Suzuki, R., and Nishiyama, A. (2011). Age-dependent fate and lineage restriction of single NG2 cells. Development *138*, 745–753.

Zlokovic, B.V. (2008). The blood-brain barrier in health and chronic neurodegenerative disorders. Neuron *57*, 178–201.